Stability Control of Electric Vehicles with Four Independently Actuated Wheels

Rongrong Wang and Junmin Wang*
Department of Mechanical and Aerospace Engineering
Ohio State University, Columbus, OH 43210

Abstract — **A vehicle stability control approach for four-wheel independently actuated (4WIA) electric vehicles is presented. The proposed control method consists of a higher-level controller and a lower-level controller. Due to the possible modeling error and parametric uncertainties, an adaptive control based higher-level controller is designed to yield the vehicle virtual control efforts. The lower-level controller allocates the required control efforts to the four in-wheel motors for generating the desired tire forces. An analytic solution on how to distribute the higher-level control efforts is given, when the actuators constraints are not considered. Simulations based on a high-fidelity, CarSim®, full-vehicle model show the effectiveness of the control approach.**

I. INTRODUCTION

FOUR wheel independently-actuated (4WIA) electric vehicle is a promising vehicle architecture due to its potentials in emissions and fuel consumption reductions [1]. 4WIA electric vehicles employ four in-wheel (or hub) motors to actuate the four wheels, and the torque and driving/braking mode of each wheel can be controlled independently. Such an actuation flexibility together with the electric motors' fast and precise torque responses may enhance the existing vehicle control strategies, e.g. traction control system (TCS), direct yaw-moment control (DYC), and other advanced vehicle motion/stability control systems [2][3][4][5][20][21].

This paper considers the stability control of a 4WIA electric vehicle. Many studies have been carried out on the vehicle stability control. However, most of them are for the traditional vehicle architectures [6][7][8], not for the 4WIA electric vehicles. Sakai [9] proposed a DYC system for a 4WIA electric vehicle, but only the vehicle lateral motion was controlled. Besides, a half vehicle model which is a linear approximation of the vehicle dynamics was used. A braking control method for electric vehicle was proposed in [10], the studied vehicle was driven by independent front and rear motors, not by in-wheel motors. A stability control system for four-wheel driven hybrid electric vehicle was proposed in [11]. The vehicle was driven by a front motor and a rear motor, and the rear motor with an electro hydraulic brake was used to generate the required torque split for motion control. Thus the control problem is different from the one considered in this study.

The actuators in a 4WIA electric vehicle are more than those in a conventional vehicle. This actuation redundancy makes the 4WIA electric vehicle control problem more challenging but rewarding. The proposed control system consists of a higher-level controller and a lower-level controller. Due to the possible modeling inaccuracies and vehicle parametric uncertainties, an adaptive controller is designed as the higher-level control to give the required virtual ground forces from the left and right sides of the vehicle. The lower-level controller allocates the virtual ground forces from the higher-level controller to the four wheels. Control allocation algorithms are generally used to distribute the higher-level control signals to the lower-level actuators [5][12]. However, the numerical optimization-based control allocation algorithms usually require high computational efforts, thus may challenge the implementations in real-time. In this study, an analytic solution of allocating the ground forces is given without explicitly considering the actuators' constraints.

The rest of the paper is organized as follows. System modeling is presented in section 2. The proposed vehicle control method is described in section 3. Simulation results are given in section 4 followed by conclusive remarks.

II. SYSTEM MODELING

A schematic diagram of a vehicle model is shown in Figure 1. Vehicle equations of motion in longitudinal, lateral, and yaw directions can be expressed as:

$$\begin{cases} \dot{V}_x = V_y \Omega_z - \frac{C_a}{M} V_x^2 + \frac{1}{M} F_X \\ \dot{V}_y = -V_x \Omega_z + \frac{1}{M} F_Y \\ \dot{\Omega}_z = \frac{1}{I_z} M_z \end{cases}, \qquad (1)$$

where V_x and V_y are the vehicle longitudinal speed and lateral speed, respectively, Ω_z is the yaw rate. M is the mass of the vehicle, I_z is the yaw inertia, and C_a is the aerodynamic drag term. F_X, F_Y, and M_z are the total forces/moment represented by the summation of the tire forces generated at all the four tires, and can be written as

$$\begin{cases} F_X = \left(F_{xfl} + F_{xfr}\right)\cos\sigma - \left(F_{yfl} + F_{yfr}\right)\sin\sigma + F_{xrl} + F_{xrr} \\ F_Y = \left(F_{yfl} + F_{yfr}\right)\cos\sigma + \left(F_{xfl} + F_{xfr}\right)\sin\sigma + F_{yrl} + F_{yrr} \\ M_Z = \left(\left(F_{yfl} - F_{yfr}\right)\sin\sigma + \left(F_{xfr} - F_{xfl}\right)\cos\sigma + F_{xrr} - F_{xrl}\right)l_s \\ \qquad - \left(F_{yfr} + F_{yrr}\right)l_r + \left(\left(F_{yfr} + F_{yfl}\right)\cos\sigma + \left(F_{xfr} + F_{xfl}\right)\sin\sigma\right)l_f \end{cases}, \qquad (2)$$

with σ being the front wheel steering angle. Based on (2), (1) can be rewritten as

$$\begin{bmatrix} \dot{V}_x \\ \dot{V}_y \\ \dot{\Omega}_z \end{bmatrix} = \begin{bmatrix} V_y\Omega_z - \frac{C_a}{M}V_x^2 \\ -V_x\Omega_z \\ 0 \end{bmatrix} + B_yF_y + B_xF_x = \begin{bmatrix} f_1(X) \\ f_2(X) \\ f_3(X) \end{bmatrix} + B_xF_x, \quad (3)$$

where $F_x = \begin{bmatrix} F_{xfl} & F_{xfr} & F_{xrl} & F_{xrr} \end{bmatrix}^T$, $F_y = \begin{bmatrix} F_{yfl} & F_{yfr} & F_{yrl} & F_{yrr} \end{bmatrix}^T$ are the tire longitudinal and lateral forces. The corresponding matrices are:

$$B_x = \begin{bmatrix} \frac{\cos\sigma}{M} & \frac{\cos\sigma}{M} & \frac{1}{M} & \frac{1}{M} \\ \frac{\sin\sigma}{M} & \frac{\sin\sigma}{M} & 0 & 0 \\ \frac{l_f\sin\sigma - l_s\cos\sigma}{I_z} & \frac{l_f\sin\sigma + l_s\cos\sigma}{I_z} & \frac{-l_s}{I_z} & \frac{l_s}{I_z} \end{bmatrix},$$

$$B_y = \begin{bmatrix} \frac{-\sin\sigma}{M} & \frac{-\sin\sigma}{M} & 0 & 0 \\ \frac{\cos\sigma}{M} & \frac{\cos\sigma}{M} & \frac{1}{M} & \frac{1}{M} \\ \frac{l_f\cos\sigma + l_s\sin\sigma}{I_z} & \frac{l_f\cos\sigma - l_s\sin\sigma}{I_z} & \frac{-l_r}{I_z} & \frac{-l_r}{I_z} \end{bmatrix}.$$

Note that the tire lateral forces are functions of the tire slip angles, which can be calculated as

$$\begin{cases} \alpha_{fl} = -\sigma + \tan^{-1}\left(\frac{V_y + \Omega_z l_f}{V_y - \Omega_z l_s}\right) \\ \alpha_{fr} = -\sigma + \tan^{-1}\left(\frac{V_y + \Omega_z l_f}{V_y + \Omega_z l_s}\right) \\ \alpha_{rl} = \tan^{-1}\left(\frac{V_y - \Omega_z l_f}{V_y - \Omega_z l_s}\right) \\ \alpha_{rr} = \tan^{-1}\left(\frac{V_y - \Omega_z l_f}{V_y + \Omega_z l_s}\right) \end{cases}, \quad (4)$$

which means that the tire lateral forces F_y are also functions of the vehicle states. So we can rewrite the vehicle model as

$$\begin{cases} \dot{V}_x = f_1(X) + B_{x1}F_x \\ \dot{V}_y = f_2(X) + B_{x2}F_x \\ \dot{\Omega}_z = f_3(X) + B_{x3}F_x \end{cases}, \quad (5)$$

where B_{xi} and B_{yi} are the ith columns of B_x and B_y, and

$f_1 = V_y\Omega_z - \frac{C_a}{M}V_x^2 + B_{y1}F_y$, $f_2 = -V_x\Omega_z + B_{y2}F_y$, $f_3 = B_{y3}F_y$.

The wheel dynamics can be written as

$$I\dot{\omega}_i = T_i - \left(F_{xi} + F_{i\_roll}\right)R, \quad (6)$$

where T_i is the in-wheel motor torque. F_{i_roll} is the tire rolling resistance, which can be calculated as

$$F_{i\_roll} = F_{zi}\left(\eta_o + \eta_1 V_{xi}^2\right), \quad (7)$$

where η_o is a coefficient in the order of 10^{-2}, η_1 is a coefficient in the order of 10^{-8}, F_{zi} is the tire normal load and can be either calculated from the load transfer model or with the tire deflection [14]. The mechanical motion of a motor or a vehicle is much slower than a motor's electromagnetic dynamics, implying that the dynamic response of the motor driver and in-wheel motor can be ignored. Thus, the motor torque can be written as

$$T_i = k_i u_i, \quad (8)$$

with u_i being the motor torque control signal, and k_i being the motor control gain. As the motor torque can be obtained from the motor current or the motor control signal [16], one can assume that the motor torque is known.

The tire slip ratio is defined as

$$s_i = \frac{\omega_i R - V_i}{\max\left(\omega_i R, V_i\right)}, \quad (9)$$

with the speeds at the wheel centers being calculated by

$$\begin{cases} V_{fl} = \left(V_x - \Omega_z l_s\right)\cos\sigma + \left(V_y + \Omega_z l_f\right)\sin\sigma \\ V_{fr} = \left(V_x + \Omega_z l_s\right)\cos\sigma + \left(V_y + \Omega_z l_f\right)\sin\sigma \\ V_{rl} = V_x - \Omega_z l_s \\ V_{rr} = V_x + \Omega_z l_s \end{cases}. \quad (10)$$

Based on the above equation, the accelerations at the wheel centers can also be calculated. Global positioning system (GPS) and inertia measurement unit (IMU) have been proved to be an effective means of measuring vehicle states [17][18]. The wheel speeds can also be measured with a wheel speed sensors and the wheel angular accelerations can be estimated in real-time with a Kalman filter such as the one in [19]. Thus, in this study, we assume all of the required signals to be known.
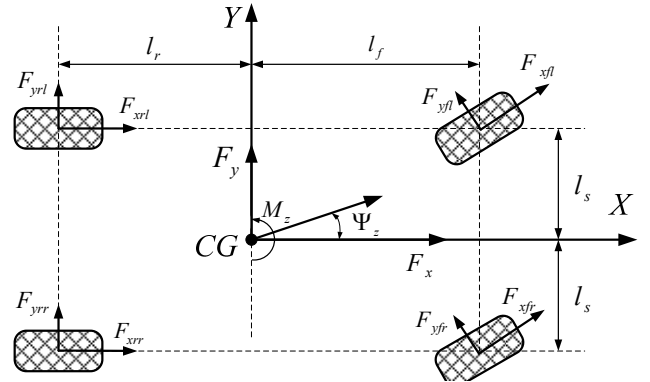

Figure 1. Schematic diagram of a vehicle model.

III. CONTROLLER DESIGN

The higher-level and lower-level controller designs are presented in this section.

A. Higher-level controller design

In this paper, we consider the vehicle longitudinal speed and yaw rate control, and thus the vehicle model can be written as

$$\begin{bmatrix} \dot{V}_x \\ \dot{\Omega}_z \end{bmatrix} = \begin{bmatrix} f_1(X) \\ f_3(X) \end{bmatrix} + \begin{bmatrix} \frac{\cos\sigma}{M} & \frac{\cos\sigma}{M} & \frac{1}{M} & \frac{1}{M} \\ \frac{l_f\sin\sigma - l_s\cos\sigma}{I_z} & \frac{l_f\sin\sigma + l_s\cos\sigma}{I_z} & \frac{-l_s}{I_z} & \frac{l_s}{I_z} \end{bmatrix}F_x. \quad (11)$$

It is known that there is a matrix N which can make the following hold,

$$\begin{bmatrix} \frac{\cos\sigma}{M} & \frac{\cos\sigma}{M} & \frac{1}{M} & \frac{1}{M} \\ \frac{l_f\sin\sigma - l_s\cos\sigma}{I_z} & \frac{l_f\sin\sigma + l_s\cos\sigma}{I_z} & \frac{-l_s}{I_z} & \frac{l_s}{I_z} \end{bmatrix} = \begin{bmatrix} \frac{1}{M} & \frac{1}{M} & \frac{1}{M} & \frac{1}{M} \\ -\frac{l_s}{I_z} & \frac{l_s}{I_z} & -\frac{l_s}{I_z} & \frac{l_s}{I_z} \end{bmatrix}N, \quad (12)$$

with N being

$$N = \begin{bmatrix} \cos\sigma - \frac{l_f\sin\sigma}{2l_s} & -\frac{l_f\sin\sigma}{2l_s} & 0 & 0 \\ \frac{l_f\sin\sigma}{2l_s} & \cos\sigma + \frac{l_f\sin\sigma}{2l_s} & 0 & 0 \\ 0 & 0 & 1 & 0 \\ 0 & 0 & 0 & 1 \end{bmatrix}.$$

Define the virtual tire force as

$$F_v = NF_x, \quad (13)$$

with $F_v = \begin{bmatrix} F_{v\_fl} & F_{v\_fr} & F_{v\_rl} & F_{v\_rr} \end{bmatrix}^T$, the vehicle model can be

rewritten as

$$\begin{bmatrix} \dot{V}_x \\ \dot{\Omega}_z \end{bmatrix} = \begin{bmatrix} f_1(X) \\ f_3(X) \end{bmatrix} + \begin{bmatrix} \frac{1}{M} & \frac{1}{M} & \frac{1}{M} & \frac{1}{M} \\ \frac{l_s}{I_z} & \frac{l_s}{I_z} & -\frac{l_s}{I_z} & \frac{l_s}{I_z} \end{bmatrix} F_v, \tag{14}$$

with $X = [V_x \ \Omega_z]^T$. One can see that the two virtual forces on the same side of the vehicle have the same effect on the vehicle longitudinal speed and yaw rate dynamics. So the total control effort of the two wheels on the same side can be written as

$$\begin{cases} F_{v\_r} = F_{v\_fr} + F_{v\_rr} \\ F_{v\_l} = F_{v\_fl} + F_{v\_rl} \end{cases}. \tag{15}$$

Based on (14) and (15), the following holds

$$\begin{bmatrix} \dot{V}_x \\ \dot{\Omega}_z \end{bmatrix} = \begin{bmatrix} f_1(X) \\ f_3(X) \end{bmatrix} + \begin{bmatrix} \frac{1}{M} & \frac{1}{M} \\ -\frac{l_s}{I_z} & \frac{l_s}{I_z} \end{bmatrix} \begin{bmatrix} F_{v\_l} \\ F_{v\_r} \end{bmatrix}. \tag{16}$$

The above vehicle model can be further written as

$$\begin{cases} \dot{V}_x = f_1(X) + \frac{1}{M} u_v \\ \dot{\Omega}_z = f_3(X) + \frac{l_s}{I_z} u_s \end{cases}, \tag{17}$$

with

$$\begin{cases} u_v = F_{v\_l} + F_{v\_r} \\ u_s = F_{v\_r} - F_{v\_l} \end{cases}. \tag{18}$$

It indicates that the vehicle speed is controlled by u_v, while the yaw rate error is compensated with the virtual force split u_s.

The higher-level controller is designed based on (17). Note that as soon as u_v and u_s are obtained, the virtual forces F_{v_r} and F_{v_l} can be calculated from (18). For the first channel, the following controller

$$u_v^* = M\left(-f_1 + K_1 e_x + \dot{V}_{rx}\right), \tag{19}$$

with V_{rx} being the reference speed and K_1 being a positive constant, can make the tracking error, $e_x = V_{rx} - V_x$, converge to 0 as $t \to \infty$. However, due to the modeling error and parameter uncertainties, $f_1(X)$ and M may not be accurately obtained, an adaptive controller is thus designed to give the u_v and u_s. The controller for the first channel is written as

$$u_v = \hat{u}_v + u_{v\_s} = \hat{M}\left(-\hat{f}_1 + K_1 e_x + \dot{V}_{rx}\right) + u_{v\_s}, \tag{20}$$

where $\hat{f}_1$ and $\hat{M}$ are the estimated values of f_1 and M, respectively. u_{v_s} is a supervisory controller. By defining $\tilde{M} = \hat{M} - M$ and $\tilde{f}_1 = \hat{f}_1 - f_1$, the first channel can be written as

$$\dot{V}_x = \left(\hat{f}_1 - \tilde{f}_1\right) + \frac{1}{M}\left(M + \tilde{M}\right)\left(-\hat{f}_1 + K_1 e_x + \dot{V}_{rx}\right) + \frac{u_{v\_s}}{M}$$

$$= \left(\left(\hat{f}_1 - \tilde{f}_1\right) + \left(-\hat{f}_1 + K_1 e_x + \dot{V}_{rx}\right)\right) + \frac{\tilde{M}}{M}\hat{u}_v + \frac{u_{v\_s}}{M} \tag{21}$$

$$= \left(-\tilde{f}_1 + K_1 e_x + \dot{V}_{rx}\right) + \frac{\tilde{M}}{M}\hat{u}_v + \frac{u_{v\_s}}{M},$$

which means that the error dynamics can be written as

$$\dot{e}_x = -K_1 e_x + \tilde{f}_1 - \frac{\tilde{M}\hat{u}_v}{M} - \frac{u_{v\_s}}{M}. \tag{22}$$

Define a Lyapunov function candidate for this channel as

$$V_1 = \frac{1}{2}\left(e_x^2 + \frac{\tilde{f}_1^2}{\gamma_1} + \frac{\tilde{M}^2}{\gamma_2 M}\right), \tag{23}$$

where γ_1, and γ_2 are positive constants. The time derivative of V_1 is

$$\dot{V}_1 = e_x \dot{e}_x + \frac{\tilde{f}_1\left(\dot{\hat{f}}_1 - \dot{f}_1\right)}{\gamma_1} + \frac{\tilde{M}\dot{\hat{M}}}{\gamma_2 M}$$

$$= e_x\left(-K_1 e_x + \tilde{f}_1 - \frac{\tilde{M}}{M}\hat{u}_v - \frac{u_{v\_s}}{M}\right) + \frac{\tilde{f}_1}{\gamma_1}\left(\dot{\hat{f}}_1 - \dot{f}_1\right) + \frac{\tilde{M}\dot{\hat{M}}}{\gamma_2 M} \tag{24}$$

$$= -K_1 e_x^2 + \left(e_x \tilde{f}_1 + \frac{\tilde{f}_1\dot{\hat{f}}_1}{\gamma_1}\right) - \left(\frac{e_x \tilde{M}\hat{u}_v}{M} - \frac{\tilde{M}\dot{\hat{M}}}{\gamma_2 M}\right) - \frac{\tilde{f}_1\dot{f}_1}{\gamma_1} - \frac{e_x u_{v\_s}}{M}.$$

If the following holds

$$\begin{cases} \dot{\hat{f}}_1 = -\gamma_1 e_x \\ \dot{\hat{M}} = e_x \gamma_2 \hat{u}_v \end{cases}, \tag{25}$$

and assuming that the upper bound of $\hat{f}_1$ has the same bound of f_1, the time derivative of V_1 can be written as

$$\dot{V}_1 = -K_1 e_x^2 - \frac{\tilde{f}_1\dot{f}_1}{\gamma_1} - \frac{e_x u_{v\_s}}{M}$$

$$\leq -K_1 e_x^2 + \frac{|\hat{f}_1 - f_1||\dot{f}_1|}{\gamma_1} - \frac{e_x u_{v\_s}}{M} \tag{26}$$

$$\leq -K_1 e_x^2 + \frac{\left(f_{1\_max} - f_{1\_min}\right)|\dot{f}_1|_{max}}{\gamma_1} - \frac{e_x u_{v\_s}}{M}$$

where $|\dot{f}_1|_{max}$ is the upper bound of $|\dot{f}_1|$, f_{1_min} and f_{1_max} are the upper and lower bounds of f_1, respectively. One can see from (26) that if we do not use the supervisory control, $u_{v\_s} = 0$, the error can be bounded as

$$e_x^2 \leq \frac{\left(f_{1\_max} - f_{1\_min}\right)|\dot{f}_1|_{max}}{K_1 \gamma_1}. \tag{27}$$

Note that the control error e_x can be arbitrarily small as K_1 can be chosen to be arbitrarily large. If $|e_x| \geq \bar{e}_x$ with $\bar{e}_x$ being a positive value, the supervisory controller u_{v_s} can be designed as

$$u_{v\_s} = \frac{\left(f_{1\_max} - f_{1\_min}\right)|\dot{f}_1|_{max} M_{max}}{\gamma_1 e_x}, \tag{28}$$

where M_{max} is the upper bound of M. Then we have

$$\frac{\left(f_{1\_max} - f_{1\_min}\right)|\dot{f}_1|_{max}}{\gamma_1} - \frac{e_x u_{v\_s}}{M} \leq 0, \tag{29}$$

which means

$$\dot{V}_1 \leq -K_1 e_x^2 + \left(\frac{\left(f_{1\_max} - f_{1\_min}\right)|\dot{f}_1|_{max}}{\gamma_1} - \frac{e_x u_{v\_s}}{M}\right) \leq 0. \tag{30}$$

Based on the above equation, one has

$$\int_0^t K_1 e_x^2 dt \leq -\int_0^t \dot{V}_1 dt + \int_0^t \left[\frac{\left(f_{1\_max} - f_{1\_min}\right)|\dot{f}_1|_{max}}{\gamma_1} - \frac{e_x u_{v\_s}}{M}\right] dt$$

$$= V_{10} - V_1(t) + \int_0^t \left[\frac{\left(f_{1\_max} - f_{1\_min}\right)|\dot{f}_1|_{max}}{\gamma_1} - \frac{e_x u_{v\_s}}{M}\right] dt \tag{31}$$

$$\leq V_{10} - V_1(t),$$

where V_{10} is the initial value of $V_1(t)$. Based on (30), one has

$$V_{10} \geq V_1(t), \tag{32}$$

which means

$$\int_0^t e_x^2 dt \leq c, \tag{33}$$

where c is a positive constant. Note that when $|e_x| \geq \overline{e}_x$, all the signals on the right side of (22) are bounded, so $\dot{e}_x \in L_\infty$. Thus, based on the Barbalat's Lemma, it can be concluded that e_x will tend to converge to zero until $e_x < \overline{e}_x$ is satisfied [13][15]. Thus, the final controller can be written as

$$
\begin{cases}
\dot{\hat{f}}_1 = -\gamma_1 e_x \\
\dot{\hat{M}} = e_x \gamma_2 \hat{u}_v \\
u_v = \hat{u}_v + u_{v\_s} \\
\hat{u}_v = \hat{M}\left(-\hat{f}_1 + K_1 e_x + \dot{V}_{rx}\right) \\
u_{v\_s} = \frac{\left(f_{1\_max} - f_{1\_min}\right)\left|\dot{\hat{f}}_1\right|_{max} M_{max}}{\gamma_1 e_x}, \quad \left(|e_x| \geq \overline{e}_x\right)
\end{cases}
\tag{34}
$$

The adaption law (25) may cause the control signals grow out of the boundary. Thus the following parameter update law modifications are introduced as

$$
\begin{cases}
u_v = \hat{u}_v + u_{v\_s} \\
\hat{u}_v = \hat{M}\left(-\hat{f}_1 + K_1 e_x + \dot{V}_{rx}\right)
\end{cases},
\tag{35}
$$

$$
\begin{cases}
\dot{\overline{f}}_1 = -\gamma_1 e_x - \kappa_1\left(\overline{f}_1 - \hat{f}_1\right) \\
\dot{\overline{M}} = e_x \gamma_2 \hat{u}_v - \kappa_2\left(\overline{M} - \hat{M}\right)
\end{cases},
\tag{36}
$$

where κ_1 and κ_2 are positive constants and

$$
\hat{f}_1 = \begin{cases}
\overline{f}_1 & if \ f_{1\_min} \leq \overline{f}_1 \leq f_{1\_max} \\
f_{1\_min} & if \ \overline{f}_1 < f_{1\_min} \\
f_{1\_max} & if \ \overline{f}_1 > f_{1\_max}
\end{cases},
\tag{37}
$$

$$
\hat{M} = \begin{cases}
\overline{M} & if \ M_{min} \leq \overline{M} \leq M_{max} \\
M_{min} & if \ \overline{M} < M_{min} \\
M_{max} & if \ \overline{M} > M_{max}
\end{cases}.
\tag{38}
$$

Redefine the Lyapunov function candidate (23) as

$$
V_{1\_new} = \frac{1}{2}\left(e_x^2 + \frac{\left(\overline{f}_1 - f_1\right)^2 - \left(\overline{f}_1 - \hat{f}_1\right)^2}{\gamma_1} + \frac{\left(\overline{M} - M\right)^2 - \left(\overline{M} - \hat{M}\right)^2}{\gamma_2 M}\right).
\tag{39}
$$

Based on (35) and (36), the time derivative of the above Lyapunov function candidate is

$$
\begin{aligned}
\dot{V}_{1\_new} &= e_x\left(-K_1 e_x + \tilde{f}_1 - \frac{\tilde{M}}{M}\hat{u}_v - \frac{u_{v\_s}}{M}\right) \\
&+ \frac{\left(\overline{f}_1 - f_1\right)\left(\dot{\overline{f}}_1 - \dot{f}_1\right) - \left(\overline{f}_1 - \hat{f}_1\right)\left(\dot{\overline{f}}_1 - \dot{\hat{f}}_1\right)}{\gamma_1} + \frac{\left(\overline{M} - M\right)\dot{\overline{M}} - \left(\overline{M} - \hat{M}\right)\left(\dot{\overline{M}} - \dot{\hat{M}}\right)}{\gamma_2 M} \\
&= -K_1 e_x^2 + \frac{\gamma_1 e_x\left(\hat{f}_1 - f_1\right) - \overline{f}_1 \dot{\hat{f}}_1 - f_1 \dot{\overline{f}}_1 + f_1 \dot{\hat{f}}_1 + \overline{f}_1 \dot{\hat{f}}_1 + \hat{f}_1 \dot{\overline{f}}_1 - \hat{f}_1 \dot{\hat{f}}_1}{\gamma_1} \\
&+ \frac{-e_x \gamma_2\left(\hat{M} - M\right)\hat{u}_v - M\dot{\overline{M}} + \hat{M}\dot{\overline{M}} + \overline{M}\dot{\hat{M}} - \hat{M}\dot{\hat{M}}}{\gamma_2 M} - \frac{e_x u_{v\_s}}{M} \\
&= -K_1 e_x^2 + \frac{\left(\gamma_1 e_x + \dot{\hat{f}}_1\right)\left(\hat{f}_1 - f_1\right) + \left(\overline{f}_1 - \hat{f}_1\right)\dot{\hat{f}}_1}{\gamma_1} \\
&+ \frac{\left(\dot{\overline{M}} - e_x \gamma_2 \hat{u}_v\right)\left(\hat{M} - M\right) + \left(\overline{M} - \hat{M}\right)\dot{\overline{M}}}{\gamma_2 M} + \frac{\left(f_1 - \overline{f}_1\right)\dot{f}_1}{\gamma_1} - \frac{e_x u_{v\_s}}{M}.
\end{aligned}
\tag{40}
$$

Based on (36) and (37), if $f_{1\_min} \leq \overline{f}_1 \leq f_{1\_max}$, the following holds

$$
\hat{f}_1 = \overline{f}_1, \quad \dot{\overline{f}}_1 = \gamma_1 e_x.
\tag{41}
$$

And if $\overline{f}_1 < f_{1\_min}$ or $\overline{f}_1 > f_{1\_max}$, we have

$$
\begin{cases}
\dot{\hat{f}}_1 = 0 \\
\left(\gamma_1 e_x + \dot{\hat{f}}_1\right)\left(\hat{f}_1 - f_1\right) = -\kappa_1\left(\overline{f}_1 - \hat{f}_1\right)\left(\hat{f}_1 - f_1\right) \leq 0
\end{cases},
\tag{42}
$$

which means the following will always hold

$$
\frac{\left(\gamma_1 e_x + \dot{\hat{f}}_1\right)\left(\hat{f}_1 - f_1\right) + \left(\overline{f}_1 - \hat{f}_1\right)\dot{\hat{f}}_1}{\gamma_1} \leq 0.
\tag{43}
$$

Similarly, one has

$$
\frac{\left(\dot{\overline{M}} - e_x \gamma_2 \hat{u}_v\right)\left(\hat{M} - M\right) + \left(\overline{M} - \hat{M}\right)\dot{\overline{M}}}{\gamma_2 M} \leq 0.
\tag{44}
$$

So (40) can be rewritten as

$$
\dot{V}_{1\_new} \leq -K_1 e_x^2 + \frac{\left(f_1 - \overline{f}_1\right)\dot{f}_1}{\gamma_1} - \frac{e_x u_{v\_s}}{M}.
\tag{45}
$$

Based on (36), one can see that if $\overline{f}_1$ tends to move out of its boundary $[f_{1\_min}, f_{1\_max}]$, the feedback term $-\kappa_1(\overline{f}_1 - \hat{f}_1)$ will pull $\overline{f}_1$ back to $\hat{f}_1$. Thus $\overline{f}_1$ is also bounded. In order to make $\frac{\left(f_1 - \overline{f}_1\right)\dot{f}_1}{\gamma_1} - \frac{e_x u_{v\_s}}{M} \leq 0$, the supervisory controller u_{v_s} can be redesigned as

$$
u_{v\_s} = \frac{\max\left(|\overline{f}_1 - f_{1\_max}|, |\overline{f}_1 - f_{1\_min}|\right)\left|\dot{f}_1\right|_{max} M_{max}}{\gamma_1 e_x}.
\tag{46}
$$

Thus, the final modified control law for the first channel is given by (35), (36), (37), (38), and (46).

If we define the Lyapunov function candidate for the second channel as

$$
V_2 = \frac{1}{2}\left(e_\Omega^2 + \frac{\left(\overline{f}_3 - f_3\right)^2 - \left(\overline{f}_3 - \hat{f}_3\right)^2}{\gamma_3} + \frac{\left(\overline{I}_z - I_z\right)^2 - \left(\overline{I}_z - \hat{I}_z\right)^2}{\gamma_4 I_z}\right),
\tag{47}
$$

where $e_\Omega = \Omega_{rz} - \Omega_z$, κ_3 and κ_4 are positive constants and

$$
\begin{cases}
\dot{\overline{f}}_3 = -\gamma_3 e_\Omega - \kappa_3\left(\overline{f}_3 - \hat{f}_3\right) \\
\dot{\overline{I}}_z = e_\Omega l_s \gamma_4 \hat{u}_s - \kappa_4\left(\overline{I}_z - \hat{I}_z\right)
\end{cases},
\tag{48}
$$

$$
\hat{f}_3 = \begin{cases}
\overline{f}_3 & if \ f_{3\_min} \leq \overline{f}_3 \leq f_{3\_max} \\
f_{3\_min} & if \ \overline{f}_3 < f_{3\_min} \\
f_{3\_max} & if \ \overline{f}_3 > f_{3\_max}
\end{cases},
\tag{49}
$$

$$
\hat{I}_z = \begin{cases}
\overline{I}_z & if \ I_{z\_min} \leq \overline{I}_z \leq I_{z\_max} \\
I_{z\_min} & if \ \overline{I}_z < I_{z\_min} \\
I_{z\_max} & if \ \overline{I}_z > I_{z\_max}
\end{cases}.
\tag{50}
$$

Here, f_{3_min} and f_{3_max} are the upper and lower bounds of f_3, respectively. I_{z_min} and I_{z_max} are the lower and upper bounds of I_z. Similar to the controller design for the first channel, the control law for the second channel can also be designed as

$$
\begin{cases}
u_s = \hat{u}_s + u_{s\_s} \\
\hat{u}_s = \frac{\hat{I}_z\left(-\hat{f}_3 + K_2 e_\Omega + \dot{\Omega}_{rx}\right)}{l_s} \\
u_{s\_s} = \frac{\max\left(|\overline{f}_3 - f_{3\_max}|, |\overline{f}_3 - f_{3\_min}|\right)\left|\dot{f}_3\right|_{max} I_{z\_max}}{l_s \gamma_3 e_\Omega}, \quad \left(|e_\Omega| \geq \overline{e}_\Omega\right)
\end{cases},
\tag{51}
$$

where $|\dot{f}_3|_{max}$ is the upper bound of $|\dot{f}_3|$.

B. Lower-level controller design

The lower-level controllers operate the four in-wheel motors to give the desired tire forces. Define the cost function as

$$
J = w_{fl} F_{xfl}^2 + w_{fr} F_{xfr}^2 + w_{rl} F_{xrl}^2 + w_{rr} F_{xrr}^2,
\tag{52}
$$

where w_i is the weighting factor for each tire force. Based on (13), the relationship between the actual tire force and the virtual tire force can be written as

$$F_x = N^{-1}F_v \qquad (53)$$

with

$$N^{-1} = \begin{bmatrix} \frac{1}{\cos\sigma} + \frac{l_f\sin\sigma}{2l_s\cos^2\sigma} & \frac{l_f\sin\sigma}{2l_s\cos^2\sigma} & 0 & 0 \\ -\frac{l_f\sin\sigma}{2l_s\cos^2\sigma} & \frac{1}{\cos\sigma} - \frac{l_f\sin\sigma}{2l_s\cos^2\sigma} & 0 & 0 \\ 0 & 0 & 1 & 0 \\ 0 & 0 & 0 & 1 \end{bmatrix}.$$

Rewrite (15) as

$$\begin{cases} F_{v\_fl} = aF_{v\_l} \\ F_{v\_rl} = (1-a)F_{v\_l} \\ F_{v\_fr} = bF_{v\_r} \\ F_{v\_rr} = (1-b)F_{v\_r} \end{cases}. \qquad (54)$$

Based on (53) and (54), the cost function (52) can be written in a function of a and b as

$$J(a,b) = w_{fl}\left((p+q)aF_{v\_l} + qbF_{v\_r}\right)^2 + w_{rl}(1-a)^2 F_{v\_l}^2 \qquad (55)$$
$$+ w_{fr}\left((p-q)bF_{v\_r} - qaF_{v\_l}\right)^2 + w_{rr}(1-b)^2 F_{v\_r}^2,$$

with $p = \frac{1}{\cos\sigma}, q = \frac{l_f\sin\sigma}{2l_s\cos^2\sigma}$. If we assume that the four weighting factors to be the same, the following will hold

$$\begin{cases} \frac{\partial J}{\partial a} = 2a\left((p+q)^2 + q^2 + 1\right)F_{v\_l}^2 + 4q^2 bF_{v\_r}F_{v\_l} - 2F_{v\_l}^2 \\ \frac{\partial J}{\partial b} = 2b\left((p-q)^2 + q^2 + 1\right)F_{v\_r}^2 + 4q^2 aF_{v\_r}F_{v\_l} - 2F_{v\_r}^2 \end{cases}, \qquad (56)$$

Based on (56), one has

$$\frac{\partial^2 J}{\partial a^2} > 0, \quad \frac{\partial^2 J}{\partial a^2}\frac{\partial^2 J}{\partial b^2} - \left(\frac{\partial^2 J}{\partial b\partial a}\right)^2 > 0, \qquad (57)$$

which means that (55) has a global minimal point when

$$\begin{cases} a = \frac{\left((p-q)^2 + q^2 + 1\right)F_{v\_l} - 2q^2 F_{v\_r}}{\left((p^2+1)^2 + 4q^2\right)F_{v\_l}} \\ b = \frac{\left((p+q)^2 + q^2 + 1\right)F_{v\_r} - 2q^2 F_{v\_l}}{\left((p^2+1)^2 + 4q^2\right)F_{v\_r}} \end{cases}. \qquad (58)$$

Note that when the steering angle is zero, $a = b = 0.5$, which means that the driving force will be equally distributed to the left or right sides of the vehicle. Also note that the constraints of the tire forces are not explicitly considered in the above optimization method.

The tire force model and the tire-road friction coefficient (TRFC) will be needed if the tire force is controlled by slip ratio feedback. However, it is usually difficult to get an accurate tire model and TRFC. In this study, the motor control signal for each motor is calculated from the wheel dynamics and can be written as

$$u_{i\_m} = \frac{I\dot{\omega}_i + \left(F_{xi\_desire} + F_{i\_roll}\right)R}{k_i}, \qquad (59)$$

where u_{i_m} is the motor control signal, F_{xi_desire} is the desired tire force calculated from (53), (54), and (58). Due to the possible measurement noises in ω_i, $\dot{\omega}_i$ cannot be directly calculated from ω_i by taking the derivative of ω_i, so the wheel angular accelerations need to be estimated/filtered before calculating the motor control signal in practice. Note that if the required tire force is greater than the maximal value, some skid/spin controller can be used to control the slip ratio such as the maximal tire force can be provided [9][10].

IV. SIMULATION STUDIES

Two simulation cases based on a high-fidelity, full-vehicle model constructed in CarSim® were conducted. The vehicle parameters in the simulations are taken from an actual prototyping 4WIA electric vehicle with in-wheel motors developed in the authors' group at The Ohio State University [16].

A. Acceleration on a Split-μ Road

In this simulation, a split-μ road was used and the vehicle steering angle was set as zero. At 1s the vehicle ran onto the split-μ road surface. The desired vehicle speed was accelerated from 50km/h to 62km/h in 6 seconds. The TRFC on the left side of the road was set as 0.8 and the right side TRFC was chosen as 0.1.
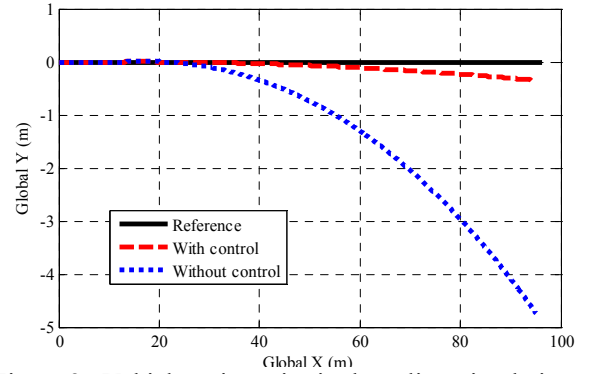

Figure 2. Vehicle trajectories in the split-μ simulation.

The vehicle global trajectories are compared in Figure 2. To better show the effectiveness of the proposed controller, the performance of an uncontrolled vehicle which runs on the same road was also compared. One can see the proposed control system can control the vehicle well, while the uncontrolled vehicle failed to follow the references as the right side wheels failed to provide the required tire forces. The vehicle yaw rates are shown in Figure 3. One can see that the controlled vehicle could follow the reference very well.
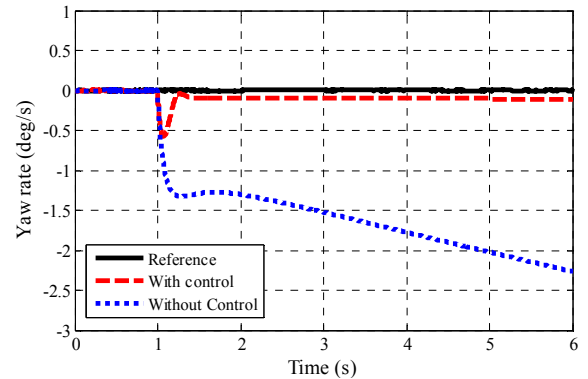

Figure 3. Yaw rates in the split-μ simulation.

B. *J-turn on Low-μ Road*

In this simulation, the vehicle ran at a constant speed of 70km/h on a low μ road. The TRFC was set to 0.4 and a counter-clockwise turn was introduced at 1.1s to make the front wheel steering angle be 1.6 degree. As the designed controller does not depend on the vehicle parameters, we set the initial vehicle mass in the controller as 600 kg, which is different to the actual vehicle mass. The vehicle yaw inertia initial value in the controller was set as 300 kg.m^2, while the real yaw inertia in the CarSim® model was 447.6 kg.m^2. The vehicle yaw rates are compared in Figure 4. One can see that the controlled vehicle followed the reference well, while the yaw rate of the uncontrolled vehicle diverted from the reference very fast. The vehicle trajectories after 4s are shown in Figure 5, where we can see again that the stability of the controlled vehicle was ensured.
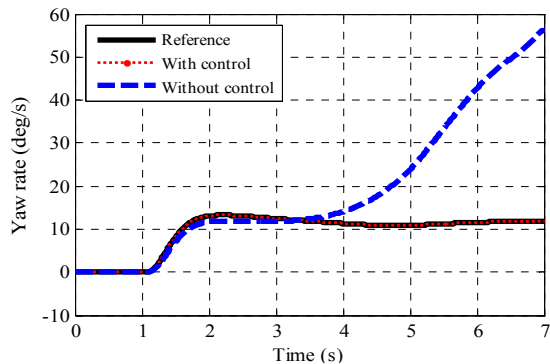

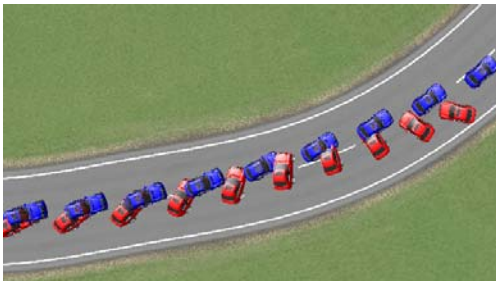Figure 4. Yaw rates in the J-turn simulation.

Figure 5. Vehicle trajectories in the J-turn simulation (red: uncontrolled vehicle; blue: controlled vehicle).

V. CONCLUSIONS

A vehicle stability control system for a 4WIA electric vehicle is presented. The proposed control method does not need the accurate vehicle parameters or tire force models but still can control the vehicle to follow the desired trajectories. An analytic solution was found to distribute the required control efforts from the higher-level controller to the four wheels without explicit considerations on actuator constraints. Simulations using a high-fidelity, CarSim®, full-vehicle model show the effectiveness of the control approach. Tire force constraints are not explicitly considered in the proposed tire force distribution design and will be incorporated in the future study.

REFERENCES

[1] C.C., Chan, "The state of the art of electric and hybrid vehicles," Proceedings of the IEEE, Vol. 95, No 4, pp. 704 – 718, April 2007.

[2] J. Yamakawa, A. Kojimaa and K. Watanabe, "A method of torque control for independent wheel drive vehicles on rough terrain," Journal of Terramechanics, Vol. 44, No 5, pp. 371-381, Nov. 2007.

[3] M. Shino, M. Nagai. "Independent wheel torque control of small-scale electric vehicle for handling and stability improvement," JSAE Review, Volume 24, Issue 4, pp. 449-456, Oct. 2003.

[4] Rongrong Wang and Junmin Wang. "Fault-Tolerant Control for Electric Ground Vehicles with Independently-Actuated In-Wheel Motors," ASME Transactions Journal of Dynamic Systems, Measurement, and Control (in press), 2011.

[5] J. Wang and R. G. Longoria, "Coordinated and Reconfigurable Vehicle Dynamics Control," IEEE Transactions on Control Systems Technology, Vol. 17, No. 3, pp. 723 – 732, 2009.

[6] H. E. Tseng, B. Ashrafi, D. Madau, T. A. Brown, and D. Recker. "The Development of Vehicle Stability Control at Ford", IEEE/ASME Transactions on Mechatronics, Vol. 4, No. 3, pp. 223-234, September 1999.

[7] M. Canale, L. Fagiano and V. Razza, "Vehicle lateral stability control via approximated NMPC: real–time implementation and software–in–the–loop test". Proceedings of the Joint 48th IEEE Conference on Decision and Control and 28th Chinese Control Conference, pp.4596-4601, December 16-18, 2009.

[8] M. Canale, L. Fagiano, M. Milanese, and P. Borodani, "Robust vehicle yaw control using an active differential and imc techniques," Control Engineering Practice, Vol. 15, No, 18, pp. 923–941, 2007.

[9] S. Sakai, H. Sado, and Y. Hori, "Motion Control in an Electric Vehicle with Four Independently Driven In-Wheel Motors", IEEE/ASME Transactions on Mechatronics, Vol. 4, No. 1, pp. 9-16, March 1999.

[10] N. Mutoh, Y. Hayano, H. Yahagi, and K. Takita, "Electric Braking Control Methods for Electric Vehicles With Independently Driven Front and Rear Wheels" IEEE Transactions on Industrial Electronics, Vol. 54, No. 2, pp. 1168-1176, April 2007.

[11] D. Kim, S. Hwang, and H. Kim, "Vehicle Stability Enhancement of Four-Wheel-Drive Hybrid Electric Vehicle Using Rear Motor Control", IEEE Transactions on Vehicular Technology, Vol. 57, No. 2, pp. 727-735, March 2008.

[12] J. Tjønnås and T. A. Johansen, "Stabilization of Automotive Vehicles Using Active Steering and Adaptive Brake Control Allocation", IEEE Transactions on Control Systems Technology, Vol. 18, No.3, pp.545-558, May 2010.

[13] Hassan K. Khalil, Nonlinear Systems, Prentice Hall, 2002.

[14] Xiaoyu Huang and Junmin Wang, "Lightweight Vehicle Control-Oriented Modeling and Payload Parameter Sensitivity Analysis," IEEE Transactions on Vehicular Technology, Vol. 60, Issue 5, pp. 1999-2011, 2011

[15] Gang Tao, "A Simple Alternative to the Barbalat Lemma," IEEE Transactions on Automatic Control, Vol. 42, No. 5, pp. 698. May 1997.

[16] R. Wang, Y. Chen, D. Feng, X. Huang, and J. Wang, "Development and Performance Characterization of an Electric Ground Vehicle with Independently Actuated In-Wheel Motors," Journal of Power Sources, Vol. 196, No. 8, pp. 3962–3971, 2011.

[17] S. Di Cairano and H.E. Tseng. "Driver-assist steering by active front steering and differential braking: design, implementation and experimental evaluation of a switched model predictive control approach," Proceedings of the 49th IEEE Conference on Decision and Control, pp. 2886 – 2891, Dec. 2010.

[18] J. Wang, L. Alexander and R. Rajamani, "Friction Estimation on Highway Vehicles Using Longitudinal Measurements," ASME Transactions Journal of Dynamic Systems, Measurement, and Control, Vol. 126, Issue 2, pp. 265 – 275, June 2004.

[19] J.D. Han, Y.Q. He, and W.L. Xu. "Angular acceleration estimation and feedback control: An experimental investigation", Mechatronics 17 (2007) 524–532.

[20] Y. Chen and J. Wang, "Fast and Global Optimal Energy-Efficient Control Allocation with Applications to Over-Actuated Electric Ground Vehicles," IEEE Transactions on Control Systems Technology (in press), 2011 (DOI: 10.1109/TCST.2011.2161989).

[21] Y. Chen and J. Wang, "Adaptive Vehicle Speed Control with Input Injections for Longitudinal Motion Independent Road Frictional Condition Estimation," IEEE Transactions on Vehicular Technology, Vol. 60, No. 3, pp. 839 - 848, 2011.